Available online at www.sciencedirect.com
SCIENCE DIRECT®
Continental Shelf Research 25 (2005) 1499–1520
CONTINENTAL SHELF RESEARCH

Internal waves, solitary-like waves, and mixing on the Monterey Bay shelf

Glenn S. Carter[a,*], Michael C. Gregg[a], Ren-Chieh Lien[b]

[a]Applied Physics Laboratory and School of Oceanography, University of Washington, 1013 NE 40th Street, Seattle, WA 98105, USA
[b]Applied Physics Laboratory, University of Washington, 1013 NE 40th Street, Seattle, WA 98105, USA

Received 7 June 2004; received in revised form 5 April 2005; accepted 11 April 2005
Available online 24 June 2005

Abstract

Microstructure measurements taken on the Monterey Bay continental shelf, within 4 km of the shelf break, reveal a complex mixing environment. Depth- and time-averaged dissipation rates ($\bar{\varepsilon} = 7.4-55.8 \times 10^{-9}\,\mathrm{W\,kg^{-1}}$) and diapycnal diffusivities ($\overline{K_\rho} = 6.1-37.8 \times 10^{-5}\,\mathrm{m^2\,s^{-1}}$) were elevated above observations made over other continental shelves with no significant topography, but were below those influenced by topographic features. The close proximity of the shelf break/canyon rim, locally generated internal tides, and nonlinear internal waves all contributed to the elevated turbulence. The complex bathymetry associated with Monterey Submarine Canyon allowed an internal tide to be generated at depths greater than 1500 m, as well as at the shelf break. The observed velocity field was normally dominated by upward energy propagation from the local shelf break generated internal tide, but near low tide downward energy propagation from a surface reflection of the internal tide generated below 1500 m was observed. Turbulent dissipation rates were not well parameterized by either the open-ocean Gregg–Henyey model or the recently developed MacKinnon–Gregg shelf model. Like its application on the New England shelf, the MacKinnon–Gregg model had the correct functional dependence on shear and stratification (dissipation increasing with increasing shear and increasing stratification), however, the magnitude and range of values were too small. The most surprising finding was the presence of what we believe to be large, high-aspect-ratio, downslope-propagating nonlinear internal solitary-like waves of elevation. Upon reaching the canyon rim, these waves propagated into deep water and transformed into waves of depression. On the shelf south of the canyon, the waves of elevation accounted for 20% of the observed turbulent kinetic energy dissipation. Off the shelf, where the solitary-like waves changed to downward displacement,

*Corresponding author. Tel.: +1 206 685 9080; fax: +1 206 543 6785.
E-mail addresses: carter@apl.washington.edu (G.S. Carter), gregg@apl.washington.edu (M.C. Gregg), lien@apl.washington.edu (R.-C. Lien).

0278-4343/$ - see front matter
doi:10.1016/j.csr.2005.04.011

their average dissipation increased 10-fold to $\bar{\varepsilon} = 2.6 \times 10^{-6}\,\mathrm{W\,kg^{-1}}$, and accounted for nearly half the dissipation in the upper 150 m.

PACS: 92.10.Lq; 92.10.Ns; 92.10.Sx

Keywords: Oceanic turbulence; Mixing processes; Continental shelves; Internal waves; Solitary waves; Parameterization; USA, California, Monterey Bay; 122°W, 36.8°N

1. Introduction

Turbulent mixing on continental shelves is much more variable than in the open-ocean thermocline. Although comparatively few direct turbulence measurements have been made on the shelf, observed diapycnal diffusivities span more than four orders of magnitude from almost molecular levels to over $10^{-2}\,\mathrm{m^2\,s^{-1}}$ (Gregg et al., 1999; Gregg and Özsoy, 1999; Nash and Moum, 2001). A multitude of factors contribute to this increased turbulent variability including nearby topography, stronger tidal currents, a large percentage of the water column in the surface and bottom mixed-layers, internal tide generation, and the presence of internal solitary waves. In recent years researchers have begun examining different regimes, identifying dominant processes, and looking for ways to parameterize the dissipation (e.g. Simpson et al., 1996; Horne et al., 1996; Gregg et al., 1999; Nash and Moum, 2001; Sundermeyer and Ledwell, 2001; MacKinnon and Gregg, 2003a, b).

Mixing on the continental shelf is important both locally and globally. Nutrients, sediments, freshwater, and pollutants all enter the ocean from terrestrial sources via the continental shelf. Turbulent mixing is an important process for redistributing these quantities throughout the water column (e.g. Shea and Broenkow, 1982; Horne et al., 1996; Sharples et al., 2001). On a global scale, Munk (1997) suggests that bays and inlets account for 100 GW of tidal dissipation. Using Topex/Poseidon altimetry data to constrain a numerical model, Egbert and Ray (2000) estimated that European, Northwest Australian, and Patagonian shelves each dissipate more that 100 GW.

The change of slope at the shelf break is an ideal location for barotropic-to-baroclinic energy conversion (e.g. Prinsenberg et al., 1974; Prinsenberg and Rattray, 1975; Baines, 1982; Pingree and New, 1989). Energy lost from the surface tide radiates away as internal waves, with an unknown proportion dissipated locally (Rudnick et al., 2003). Coastal solitary waves may be formed as part of this process, and appear to play a significant role in local mixing. From numerical simulations, Bogucki et al. (1997) report that up to 73% of the internal wave field energy could be in solitary waves. Ramp et al. (2004) note that the most energetic motions passing a moored array on the South China Sea continental shelf were highly nonlinear internal solitary waves. MacKinnon and Gregg (2003b) estimate that approximately 15% of their observed dissipation and 50% of the dissipation in the thermocline occurred during the passage of solitary waves.[1] Moum et al. (2003) report that within a solitary wave, diapycnal diffusivities were similar to those observed in internal hydraulic jumps.

Here, we present microstructure and acoustic data collected on the continental shelf within and at the mouth of Monterey Bay during August 1997. Section 2 outlines the experiment location and data collected. The velocity structure suggests both local and more distant internal tide generation (Section 3). The turbulence observations are described and compared to other shelf measurements in Section 4. A recently suggested turbulence scaling for shelf environments (MacKinnon and Gregg, 2003b) is compared to the Monterey Bay dissipations (Section 5). In Section 6 we suggest that turbulent backscatter features could be nonlinear internal solitary-like waves that propagated

[1] MacKinnon and Gregg (2003b) found that excluding boundary layers 75% of the dissipation occurred in the pycnocline with half of that associated with the passage of solitary waves. Fifty-five percent of the observed dissipation occurred in the unstratified bottom mixed layer.

from the shelf out over the canyon. Finally, the key findings are summarized in Section 7.

2. Location and data

Monterey Bay, located in central California, features the largest submarine canyon on the west coast of the United States. The canyon terminates within 100 m of the shore at the eastern end of the bay. Within the bay, the shelf north and south of the canyon is >10 km wide (Fig. 1a). Estimates of the barotropic tidal velocity in the bay range from $0.01\,\mathrm{m\,s^{-1}}$ (Petruncio et al., 1998) to $0.18\,\mathrm{m\,s^{-1}}$ (Breaker and Broenkow, 1994). Inflow through the canyon means that surface currents are out of the bay on flood tide (Petruncio et al., 1998).

A microstructure survey was conducted between 8 and 22 August 1997. The data collection concentrated primarily on mixing at the head of the submarine canyon (Carter and Gregg, 2002) and over a submarine fan at the mouth of Monterey Bay (Lien and Gregg, 2001). The microstructure data were collected with the loosely tethered deep Advanced Microstructure Profiler (AMP), which was cycled from the stern as the ship maintained steerage (~1 knot). The AMP measures the turbulent kinetic energy dissipation rate ε (Osborn and Crawford, 1980; Wesson and Gregg, 1994), temperature, and salinity. Following Osborn (1980), diapycnal diffusivity is given by

$$K_\rho = \frac{\gamma\varepsilon}{N^2}, \tag{1}$$

where γ is the mixing efficiency, taken to be $\leqslant 0.2$; N is the buoyancy frequency.

Although the continental shelf was not the focus of this experiment, 202 profiles separated into four spatial regions were collected on the Monterey Bay

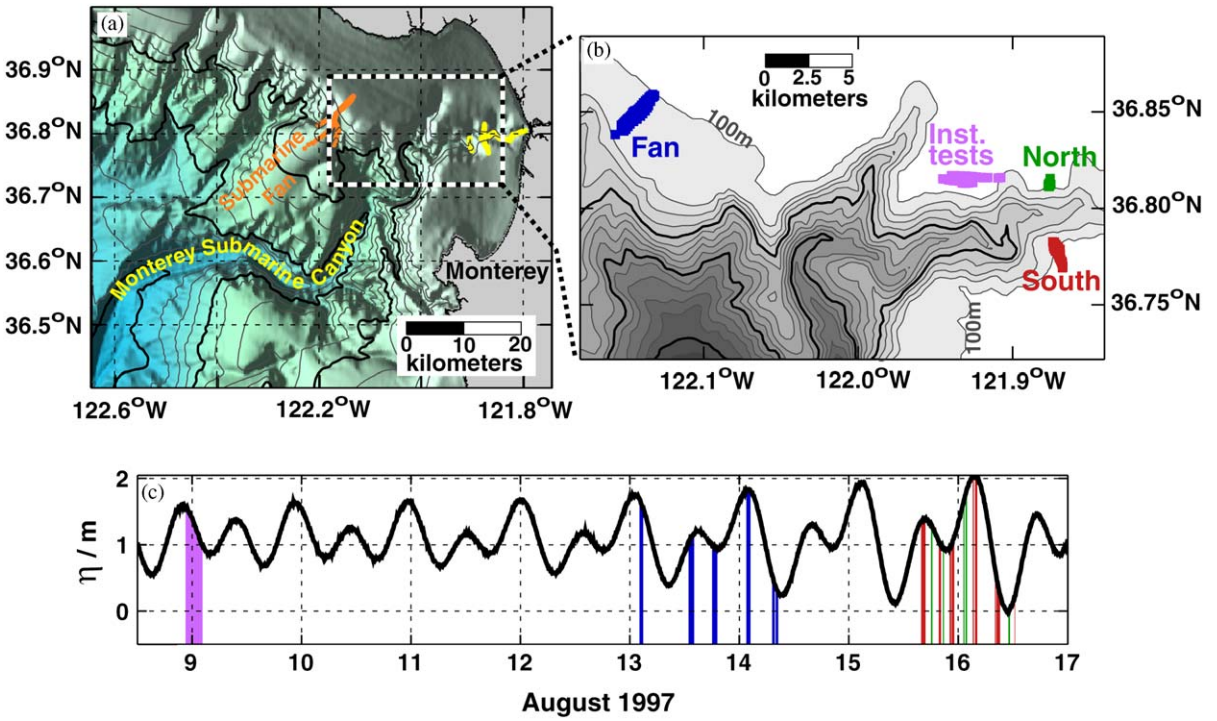

Fig. 1. (a) Map of the complex topography within and offshore of Monterey Bay. The location of the profiles analyzed in Lien and Gregg (2001) are shown in orange, and those analyzed in Carter and Gregg (2002) are plotted in yellow. Contour interval is 250 m, with the heavier lines at 1000-m intervals. (b) Detailed map showing the location of the four microstructure sampling regions on the shelf. Contour interval is 100 m, with the heavier contours marking the 500-m intervals. (c) Tidal elevation (η) with the times of the shelf microstructure profiles marked.

shelf. Apart from 38 profiles taken during instrument testing at the beginning of the experiment, all the shelf profiles were taken as part of off-shelf or cross-canyon survey lines. Eighty profiles were taken over 34 h (02:05 13 August to 12:21 14 August) on the shelf adjacent to the submarine fan at the mouth of the bay. A cross-canyon survey ($\approx$ 9 km from the canyon head) was conducted for 22 h (14:57 15 August to 12:25 16 August). Asymmetries in the shelf depth on either side of the canyon (80 m on the north rim and 120 m on the south rim) lead to significantly more profiles being taken on the southern (74) than the northern (10) shelf. Data from all four regions were within 4 km of either the shelf break or the canyon rim.

A 150-kHz broadband vessel-mounted ADCP measured water velocities below 11 m at 4-m intervals, and for most analysis an averaging interval of 3 min was used. Unfortunately, the ADCP power supply failed on 16 August; thus half of the cross-canyon surveys do not have corresponding velocity data. Acoustic images were recorded using a 200-kHz Biosonics single-beam echosounder with vertical resolution of 0.125 m. Tidal elevations were recorded at Monterey Harbor as part of the National Oceanic and Atmospheric Administration (NOAA) National Water Level Observation Network.

3. Locally generated IW field

ADCP velocity observations on and near the shelf showed a complex multilayer flow pattern. However, only the flow direction, and not the current speed, was strongly depth dependent. This pattern, consistent with a propagating internal wave, was repeated both near the submarine fan and within the bay. Complex bathymetry allowed barotropic-to-baroclinic conversion (Munk, 1997; Holloway and Merrifield, 1999) at abyssal depths as well as at the shelf break. The combination of locally and more distantly generated internal tides led to a complex internal wave field on the shelf, with both upward- and downward-propagating internal waves.

Fig. 2 shows u, v velocity components, as well as the current speed and direction ($\theta = \tan^{-1}(\frac{u}{v})$, so

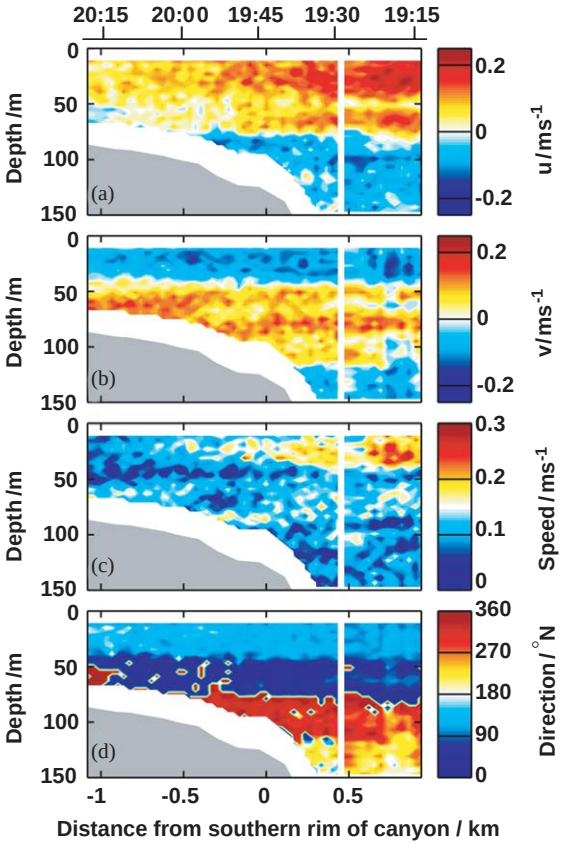

Fig. 2. ADCP velocity from the second run across the southern canyon rim (19:12 to 20:18, 15 August 1997). (a) u (east) velocity component, (b) v (north) velocity component, (c) velocity magnitude, and (d) velocity direction showing counterclockwise rotation with depth. The vertical white stripe results from an erroneous ensemble being removed.

$\theta = 0^\circ$ is north, and $\theta = 90^\circ$ is east) over the shelf south of the canyon from our second across-canyon run. These data were collected during the later portion of the minor ebb on 15 August, between 19:12 and 20:18 UTC. Magnitudes of up to $\pm 0.25\,\mathrm{m\,s^{-1}}$ were observed in both velocity components, and are consistent with our observations at other times and locations. The current speed (Fig. 2c) shows neither the two-layer structure of the u-component (Fig. 2a), nor the three-layer structure of the v-component (Fig. 2b). However, the current direction (Fig. 2d) shows counterclockwise rotation with depth. At the surface, flow was south-eastward. By 75 m depth, the flow was northward. Off the

shelf, where deeper measurements were taken, the flow was west–northwest.

Counterclockwise rotation with depth implies upward internal wave energy propagation (Leaman and Sanford, 1975; Gill, 1982), i.e. an internal wave generated or reflected off the seabed. The proximity of the shelf break and canyon rim suggests local internal tide generation. Lien and Gregg (2001) report finding a semidiurnal internal tidal beam directly off the shelf break adjacent to the submarine fan. Within Monterey Canyon fluxes were consistent with local generation (Kunze et al., 2002; Carter and Gregg, 2002). Therefore, although our shelf sampling cannot be interpreted as a time-series and does not allow an estimate of the frequency of the wave, tidal forcing seems most likely.

Over half of our velocity observations on the shelf adjacent to the submarine fan and on the southern shelf of the bay showed counterclockwise rotation. At other times, clockwise rotation or no rotation with depth was observed. Fig. 3 plots current direction versus depth for the six runs on the shelf above the fan and the four runs on the southern shelf that had ADCP data. These profiles were calculated using vector averaged velocity just beyond the shelf break, as the directions were similar to those over the shelf and this approached minimized the influence of averaging different amounts of data. For the submarine fan, runs 1, 4, and to a lesser extent 3, showed a counterclockwise rotation with depth. Run 5, which was at high water, had little rotation with depth, except for a region of counterclockwise rotation between 75 and 100 m. The remaining two runs (6 and 7), which occurred near low water, had both regions of clockwise and counterclockwise rotation. Run 6 was clockwise above $\approx$ 50 m, and run 7 clockwise between 40 and 120 m. On the southern rim of the canyon, the first three runs (labeled A, B, C) showed counterclockwise rotation with depth. The fourth run (D), which was at the beginning of flood tide, showed counterclockwise rotation in the upper half of the water column and clockwise rotation with depth below 80 m.

Downward-propagating internal waves can be generated by critical topography higher in

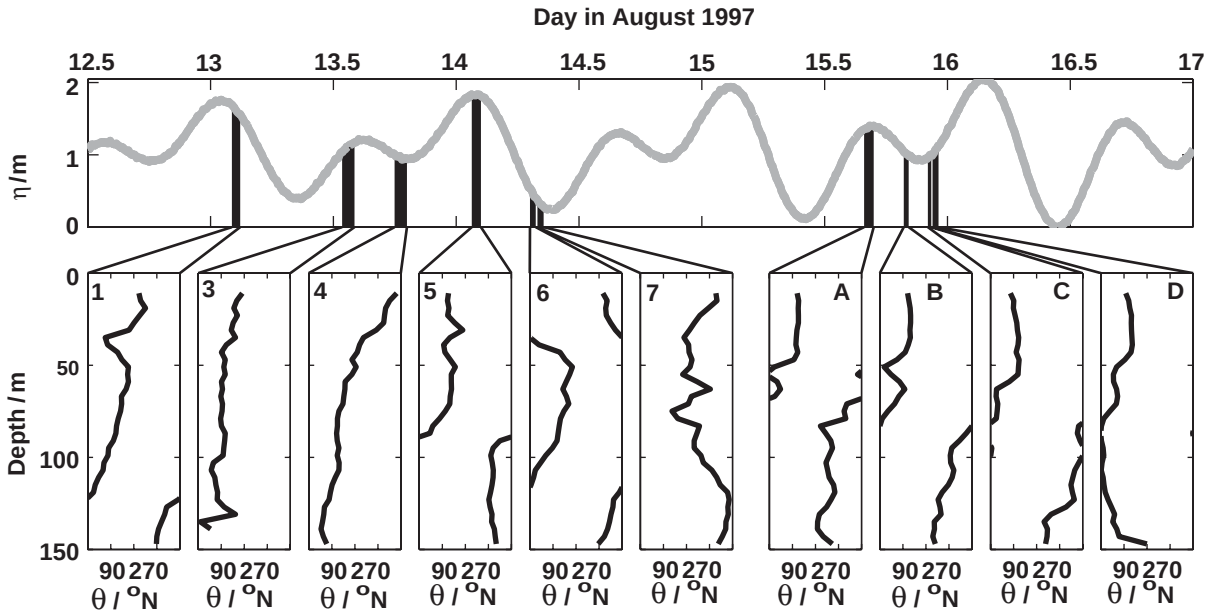

Fig. 3. Profiles of velocity direction, showing the majority of runs were dominated by counterclockwise rotation with depth (1,3,4,A,B,C). Near low water the observations were a mixture of clockwise and counterclockwise rotation. Panels 1, 3–7 are runs across the shelf at the submarine fan and A–D are from the southern canyon rim. The numbering on the submarine fan runs was chosen to be consistent with Lien and Gregg (2001). The top panel shows the location of the runs with respect to tidal elevation (η). Only the first four runs across the southern canyon shelf had ADCP observations due to a power-supply failure.

shallower water, or by either reflection or generation at the surface. The clockwise rotation in run D was below the shelf break depth, and therefore may be indicative of local generation. However, the downward-propagation in runs 6 and 7 is above the shelf level, and therefore must have been generated or reflected at the surface. As there were no strong wind-forcing events (Carter and Gregg, 2002), the most likely source of the downward propagation would be surface reflection from a remote generation site. Petruncio et al. (1998) conclude that an internal tide is generated between 1000- and 1500-m depth on the submarine fan (Fig. 1a).

Kunze et al. (2002) find no evidence to support this and suggest the internal tides are generated deeper on the complex bathymetry associated with the submarine canyon. Internal tides generated offshore and focused by coastal topography would also be consistent with their data. Numerical models suggest generation at the base of the submarine fan (O. Fringer, pers. comm.). Therefore, a possible interpretation of our data is that the incoming barotropic tide generates an internal tide deep on the submarine fan or canyon, then a second internal tide is generated as the barotropic tide passes over the shelf break or canyon rim. The incoming deeply generated internal tide reflects off the surface inshore of its generation region and propagates downward on to the shelf.

4. Observed mixing

Observed turbulent kinetic energy dissipation rates on the shelf ranged from $<10^{-10}$ to $\approx 10^{-5}\,\mathrm{W\,kg^{-1}}$. Diapycnal diffusivity[2] ranged over six orders of magnitude from $10^{-7}\,\mathrm{m^2\,s^{-1}}$. Considerable variability was observed on the shelf, both in magnitude and depth distribution. Spatially as well as temporally varying environment factors appeared to be important.

Table 1
Mean dissipation rates and diapycnal diffusivities observed in the four shelf regions

Region	$\bar{\varepsilon}$ W kg^{-1}	95% conf. int. W kg^{-1}
Test	7.4×10^{-9}	$[6.1-9.0]\times10^{-9}$
Fan	52.9×10^{-9}	$[44.6-63.8]\times10^{-9}$
North	49.1×10^{-9}	$[38.3-60.8]\times10^{-9}$
South	55.8×10^{-9}	$[49.0-63.9]\times10^{-9}$
Region	$\overline{K_\rho}$ m^2 s^{-1}	95% conf. int. m^2 s^{-1}
Test	6.1×10^{-5}	$[4.3-8.8]\times10^{-5}$
Fan	27.0×10^{-5}	$[18.7-39.5]\times10^{-5}$
North	14.1×10^{-5}	$[10.6-17.9]\times10^{-5}$
South	37.8×10^{-5}	$[32.7-44.8]\times10^{-5}$

Data within the surface and bottom mixed-layers has been excluded. The 95% bootsrapped confidence intervals on the means are also given.

4.1. Average mixing

Mean ε and K_ρ values for the instrument test drops are about five times lower than the other three regions (Table 1). The surface and bottom mixed-layers, which are defined using $\Delta\sigma_\theta = 0.01\,\mathrm{kg\,m^{-3}}$, have been excluded from this analysis. The presence and thickness of the bottom mixed-layer was highly variable, but the surface mixed-layer was generally shallower than 10 m. It is unclear why the mixing observed during the test drops were much lower than other sites, although there are two notable environmental differences. The test drops occurred during neap tide (Fig. 1c), and the density structure (Fig. 4) was consistent with coastal upwelled water propagating into the bay (Rosenfeld et al., 1994; Carter and Gregg, 2002).

Averaged profiles of stratification (N^2), shear variance (S^2), diapycnal diffusivity (K_ρ), and dissipation rate (ε) for the four shelf locations are presented in Fig. 5b–i. In order to best represent the distribution of N^2 and S^2, the means and standard deviations were calculated in loga-

[2]When calculating diapycnal diffusivity (1), the stratification used should represent the local background density field. The short spatial scales associated with shelf break processes combined with our irregular profile spacing meant time averaging the stratification was not possible. Consequently, K_ρ values in this paper were calculated with stratification derived from a single density profile resort to be monotonically increasing with depth. The diapycnal diffusivities were calculated over 1-m vertical intervals.

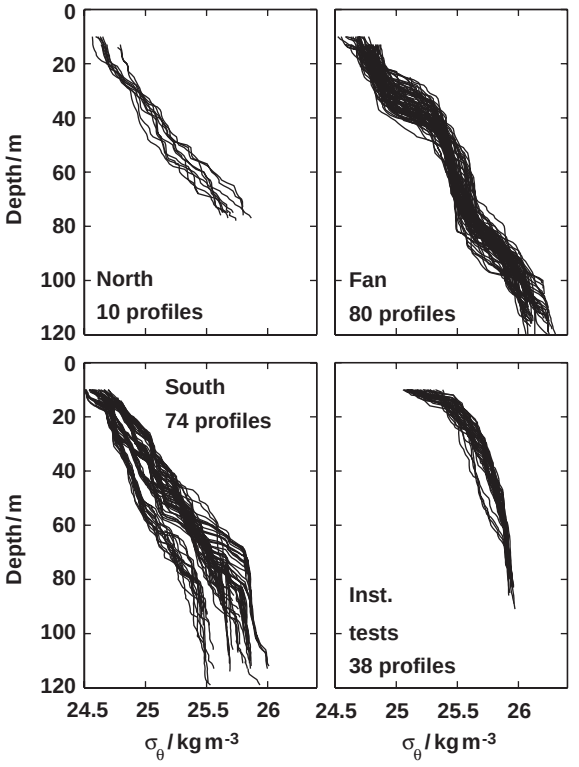

Fig. 4. Density profiles from each of the four shelf regions.

rithmic space (e.g. $\overline{N^2} = 10^{\overline{\log_{10}(N^2)}}$), whereas the mixing variables (ε, K_ρ) are dominated by extreme events so we averaged the variables themselves. The shape of the stratification profiles varied between the four regions, although the average stratification was nearly constant ($\overline{N^2} = 4{-}10 \times 10^{-5}\,\mathrm{s}^{-2}$). Data taken during instrument tests showed a nearly exponential decrease in stratification, with $\overline{N^2} \approx 4 \times 10^{-4}\,\mathrm{s}^{-2}$ near the surface and $\overline{N^2} \approx 1 \times 10^{-5}\,\mathrm{s}^{-2}$ near the bed. The other three regions had nearly constant stratification with depth, although the data near

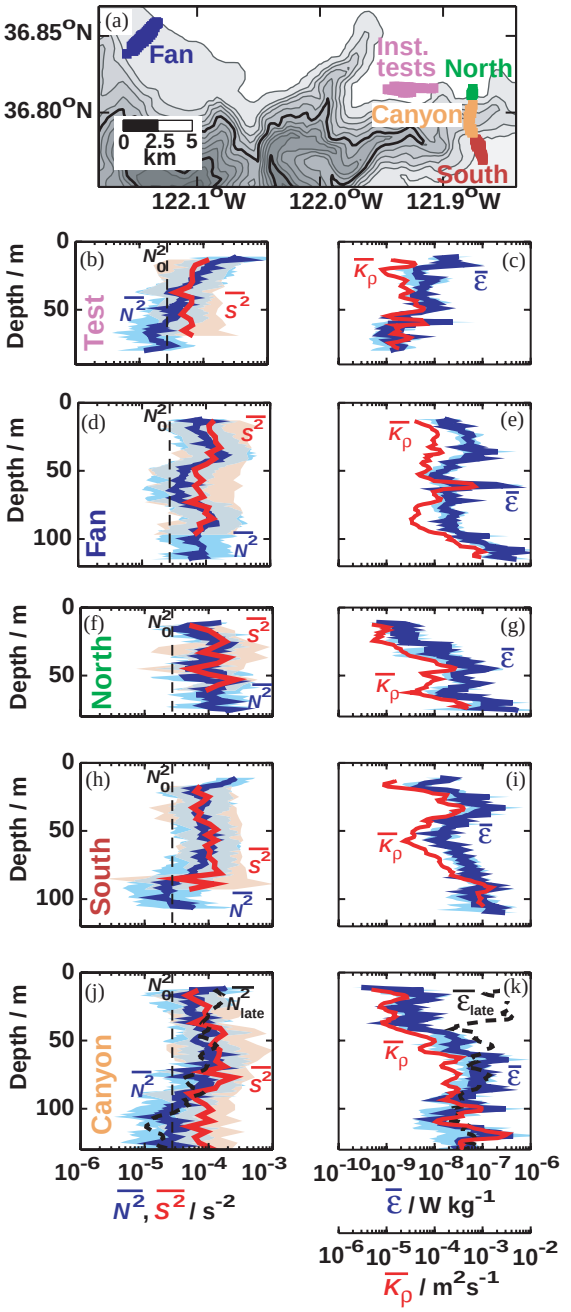

Fig. 5. Averaged profiles. (a) Locator map. (b), (d), (f), (h), and (j) show log-space-averaged 4-m shear-squared, S^2, and 1-m stratification, N^2, for the five regions. The shading gives one standard deviation either side of the mean (i.e. $\pm\sigma$). N_0^2 ($(5.2 \times 10^{-3})^2\,\mathrm{s}^{-2}$) is the GM open-ocean reference stratification. (c), (e), (g), (i), and (k) show 1-m ε and 4-m K_ρ averages. The 95% bootstrapped confidence interval on the ε averages are shaded in light blue. The canyon station is the upper 130 m from the early cross-canyon survey runs, and the black dashed line shows the later runs (see Section 4.2). The surface and bottom mixed-layers, defined by $\Delta\sigma_\theta = 0.01\,\mathrm{kg\,m^{-3}}$, were excluded from all averages.

the submarine fan had a ≈40-m thick low-stratification region at mid-depth, and the south region stratification decreased below 80 m. The 4-m first-difference shear profiles are very similar across all four regions; the test data is slightly lower in magnitude.

Averaged profiles of dissipation rate for the fan and south regions show a local maximum at 35–40 m and a near-bed increase, which starts at 100-m depth for the fan but was more gradual for the south region (starting at 60 m). The ε/K_ρ peak near 60 m in the fan average is mainly due to a single mixing event. To first order, the averaged profile of the test data showed dissipation that decreased with increasing depth. Whereas, the north region showed depth-averaged ε increasing with depth. These two regions are only 5 km apart, but sampling was separated by 7 days and the density field differed. The north, south, and fan regions all had similar near-bottom dissipation rates ($\varepsilon > 10^{-7}\,\mathrm{W\,kg^{-1}}$), however, the depth-averaged near-bed dissipation during the test drops was $\approx 2\times10^{-9}\,\mathrm{W\,kg^{-1}}$. Averaged diapycnal diffusivity showed similar patterns.

The two regions that had survey lines run multiple times (fan and south) showed variability in average mixing values between runs. Average dissipation on the shelf near the fan varied as much as 10-fold between occupations, with considerable patchiness in the location of the turbulence (not shown). Lien and Gregg (2001) report that in the water column above the submarine fan, dissipation was stronger during ebb tide. With our limited sampling (and the fact we often sampled on the shelf near slack water), we are unable to comment on any possible links between tidal phase and dissipation.

4.2. Mixing above Monterey Canyon

The last two panels in Fig. 5 give average profiles in the upper 130 m from the cross-canyon survey runs conducted ~9 km from Moss Landing (Fig. 5a). Data north of the 200-m isobath of the northern side of the canyon were disregarded due to elevated mixing from interactions with the steep topography. Primarily, Fig. 5j and k shows data from the first half of the cross-canyon survey (17:04 15 August to 00:19 16 August), however, the black dashed lines give the depth-averaged N^2 and ε profiles after the pycnocline had shallowed (04:36 to 12:05 16 August) resulting in significant changes to the average dissipation profiles.

When the pycnocline was between 50 and 80 m depth, the average near-surface dissipation ($\bar{\varepsilon}\approx 4\times10^{-10}\,\mathrm{W\,kg^{-1}}$) was lower than any of the shelf regions surveyed. Between 40 and 60 m, averaged ε increased to $\approx 10^{-7}\,\mathrm{W\,kg^{-1}}$, and below 100 m depth the isolated features associated with high acoustic backscatter (Sections 4.3 and 6) dominated the average. The stratification and shear-squared profiles are very similar to those observed on the neighboring shelves north and south of the canyon.

Once the pycnocline shallowed (dashed lines), stratification in the upper 40 m increased by a factor of about 3. The near-surface dissipation, however, increased by over two orders of magnitude to $\bar{\varepsilon}_{\mathrm{late}}\approx 3\times10^{-7}\,\mathrm{W\,kg^{-1}}$, and was larger than our other shelf observations. It appears that most of the increased near-surface dissipation occurred near the diurnal maximum high water. In their study of dissipation along the canyon axis, Carter and Gregg (2002) also found that dissipation levels increased by up to 10^2 times when the pycnocline shallowed from 120 to 50 m.

4.3. Mixing associated with isolated backscatter events

Turbulent kinetic energy dissipation rates elevated relative to the local background were observed coincident with isolated high acoustic backscatter features (Fig. 6). The tall backscatter features on the shelf (−1.5 to −1.2 km) had dissipation rates approaching $9\times10^{-7}\,\mathrm{W\,kg^{-1}}$, while above them $\varepsilon \lesssim 5\times10^{-8}\,\mathrm{W\,kg^{-1}}$. Two AMP profiles sampled through backscatter features in deeper water (0.11 and 0.47 km), and showed narrow patches of intense mixing corresponding to the backscatter. These 10-m thick patches had dissipations 10^2–10^3 times that of the surrounding water.

The features between −1.5 and −1.2 km had $\bar{\varepsilon} = 1.8\times10^{-7}\,\mathrm{W\,kg^{-1}}$ (with a 95% bootstrapped confidence interval on the mean of [1.1–2.7]

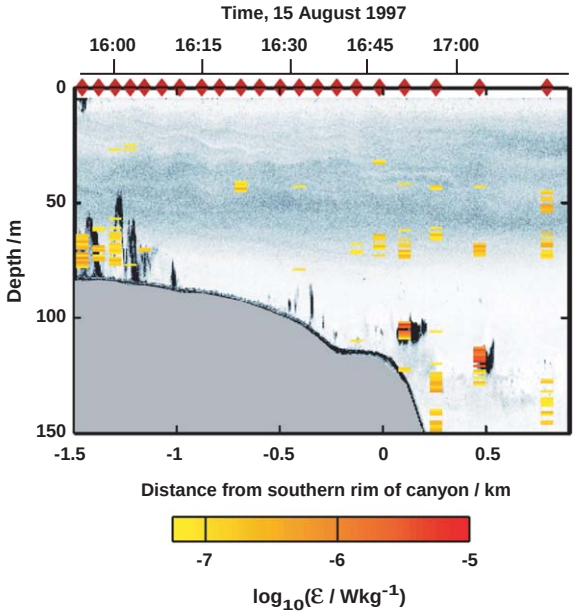

Fig. 6. Acoustic backscatter data over the southern shelf from the first cross-canyon run (15:53 to 17:14, 15 August 1997). Dissipations greater than $\log_{10}\varepsilon = -7.25$ ($\approx 5.6 \times 10^{-8}\,\mathrm{W\,kg^{-1}}$) have been overplotted, showing a correspondence between high backscatter and high dissipation. The diamonds along the top of figure show the location of AMP profiles 16537–16557.

$\times 10^{-7}\,\mathrm{W\,kg^{-1}}$), whereas those at 0.11 and 0.47 km had $\bar{\varepsilon} = 2.6 \times 10^{-6}\,\mathrm{W\,kg^{-1}}$ ($[1.8-3.5]\times 10^{-6}\,\mathrm{W\,kg^{-1}}$). Therefore, it appears that the dissipation rates associated with the offshelf backscatter features were larger than those on the shelf. However, we sample closer to the core of the offshelf features than the onshelf features so this comparison may be biased.

These features were only observed on the shelf south of the canyon during the early part of the cross-canyon survey, with the strongest features being observed during the first run. During this time the pycnocline was closer to the shelf than the surface. The first four cross-canyon runs had this deep pycnocline and continuous backscatter observations. Averaging the dissipation rates above 150 m depth from these four runs into 100 m horizontal bins, and comparing them to maximum backscatter over these four runs gives a rough estimate of the dissipation coinciding with the backscatter features. Off the shelf (i.e. $0 \leqslant$ distance $\leqslant 1.5$ km) 45% of the dissipation was associated with the backscatter features. This approach only gave that 20% of on the shelf dissipation was associated with the features. These values should be considered lower limits of the role of the backscatter features. The acoustic backscatter records are continuous, whereas, the microstructure profiles occurred at discrete times, and hence not all backscatter features had corresponding dissipation measurements, also as noted above the measurement may be at the edge of the feature. Increased dissipation associated with other boundary processes on the shelf would also help to reduce the importance of the features.

In Section 6 we speculate on the nature of these features.

4.4. Mixing compared to other shelves

Over smoothly varying continental shelf topography, microstructure and dye-release experiments have often shown that diapycnal diffusivities away from surface and bottom mixed-layers are similar to the $K_\rho \approx 10^{-5}\,\mathrm{m^2\,s^{-1}}$ observed in the open-ocean thermocline. These observations include: $K_\rho = 1-5 \times 10^{-5}\,\mathrm{m^2\,s^{-1}}$ on the Oregon Shelf (Nash and Moum, 2001); $\overline{K_\rho} = 0.5 \times 10^{-5}\,\mathrm{m^2\,s^{-1}}$ (MacKinnon and Gregg, 2003b) and $K_\rho = 0.1-1 \times 10^{-5}\,\mathrm{m^2\,s^{-1}}$ (Sundermeyer and Ledwell, 2001; Ledwell et al., 2004) on the New England shelf; and $K_\rho = 5 \times 10^{-5}\,\mathrm{m^2\,s^{-1}}$ on the Scotian shelf (Sandstrom and Oakey, 1995). Diapycnal diffusivities of $6 \times 10^{-7}\,\mathrm{m^2\,s^{-1}}$, about five times the molecular diffusivity of heat, were found on the Black Sea shelf in the absence of strong tidal and wind forcing (Gregg and Özsoy, 1999).

Small-scale topographical features and strong forcing can greatly enhance turbulent mixing on the shelf. Nash and Moum (2001) report that the presence of a 20-m high bump induced a hydraulic flow with K_ρ values of $37–170 \times 10^{-4}\,\mathrm{m^2\,s^{-1}}$. Observations in the tidal-mixing front over Georges Bank gave $K_\rho = 5-200 \times 10^{-5}\,\mathrm{m^2\,s^{-1}}$ (Horne et al., 1996). Our observations ($\overline{K_\rho} = 6-38 \times 10^{-5}\,\mathrm{m^2\,s^{-1}}$) seem to lie somewhere between the observations over smooth shelf topography and those affected by topographic features.

Internal tide generation at the nearby shelf break is the likely cause of our Monterey Bay diapycnal diffusivities being elevated above other smooth shelf observations.

Our observed turbulent kinetic energy dissipation rates ($\bar{\varepsilon} = 7.4-55.8 \times 10^{-9}\,\mathrm{W\,kg^{-1}}$) were similar to those observed on the New England shelf (MacKinnon and Gregg, 2003b), but significantly lower than dissipation rates in the Irish Sea ($\approx 10^{-6}\,\mathrm{W\,kg^{-1}}$; Simpson et al., 1996), and the Scotian shelf ($5.3 \times 10^{-7}\,\mathrm{W\,kg^{-1}}$; Sandstrom and Oakey, 1995).

Dissipation rates and diapycnal diffusivities observed on the Monterey Bay continental shelf were significantly lower than those observed in the adjacent Monterey Canyon (Fig. 1a; Carter and Gregg, 2002).

5. Dissipation scaling

Recently MacKinnon and Gregg (2003b) proposed a new scaling to estimate turbulent dissipation in coastal environments from local observations of shear and stratification. Shear (from ADCPs) and stratification (from CTDs) are commonly measured oceanic variables, and are easier to measure than microstructure. As successful parameterizations would allow for more complete global dissipation budgets and more accurate representation of dissipation in numerical simulations, we applied the MacKinnon–Gregg scaling as well as the commonly used Gregg–Henyey open-ocean scaling to our measurements to test their applicability.

Henyey et al. (1986) present a simple analytical model for turbulent kinetic energy dissipation that is in good agreement with their numerical ray-tracing experiments. Energy cascades from the energy-containing scales through the internal wave spectrum, so the dissipation rate should be related to the flux of energy (E, per unit mass) past a given (high) vertical wave number (m):

$$\varepsilon = \left\langle \frac{\partial E}{\partial m}\frac{\partial m}{\partial t} \right\rangle = \left\langle \frac{\partial E}{\partial m}\left(-\frac{\mathrm{d}\mathbf{U}}{\mathrm{d}z}\cdot\mathbf{k} \right) \right\rangle, \tag{2}$$

where $\mathbf{U}$ is the background velocity field, $\mathbf{k}$ is the wave number of the propagating wave, and $\langle * \rangle$ indicates an average over space and time scales. The form of the energy density, and hence the $\partial E/\partial m$ term, was taken to be described by the Garrett–Munk internal wave spectra (Garrett and Munk, 1972, 1975) integrated over the range of valid frequencies. Gregg (1989) modified the Henyey model to use shear, as this is the more fundamental parameter. The resulting dissipation estimate (in $\mathrm{W\,kg^{-1}}$), commonly denoted Gregg–Henyey, is

$$\varepsilon_{GH} = 1.7 \times 10^{-6} f \cosh^{-1}\left(\frac{N_0}{f}\right)\left\langle \frac{S_{10}^4}{S_{GM}^4} \right\rangle \left\langle \frac{N^2}{N_0^2} \right\rangle \tag{3}$$

$$\hookrightarrow S_{GM}^4 = 1.66 \times 10^{-10}\left(\frac{N^2}{N_0^2}\right)^2, \tag{4}$$

where $N_0 = 3\,\mathrm{cph}$, S_{10} is the observed 10-m shear, and S_{GM} is the equivalent shear from the Garrett–Munk model spectrum.

From a two-week time-series on the New England shelf, MacKinnon and Gregg (2003a) conclude that the internal wave field was not described well by the Garrett–Munk model. In particular, the modal content of the internal wave field varied considerably from day to day, to the point that, on certain days, the low modes would account for most of the shear and, a few days later, the structure would be almost entirely higher modes. MacKinnon and Gregg (2003b) start with (2), but rather than use the Garrett–Munk form of the internal wave spectrum, they used the fact that WKB-stretching (which scales the depth such that the stratification is constant) suggests $\partial E/\partial m \approx N$. They also found that the large-scale shear came mainly from near-inertial and semidiurnal waves, and consequently they used low-frequency shear (S_{lf}) in their scaling:

$$\varepsilon_{MG} = \varepsilon_0\left(\frac{N}{N_0}\right)\left(\frac{S_{lf}}{S_0}\right), \tag{5}$$

where $N_0 = S_0 = 5.2 \times 10^{-3}\,\mathrm{s^{-1}}$, and the constant, $\varepsilon_0 = 6.9 \times 10^{-10}\,\mathrm{W\,kg^{-1}}$, was chosen to give the same cruise average as the observations.

To date, the MacKinnon–Gregg scaling has only been applied on the broad New England

shelf, about halfway between the shelf break and the coast. MacKinnon and Gregg (2003b) considered data from late summer 1996, but excluded dissipations associated with the passage of solitary waves of depression, as these tended to be higher for given S^2 and N^2. They found that while both the MacKinnon–Gregg and Gregg–Henyey scalings predicted the shape of the average profile correctly, the MacKinnon–Gregg scaling predicted magnitude and variability much better. Ledwell et al. (2004), who conducted a dye-release experiment as part of the same investigation, report that the MacKinnon–Gregg scaling was consistent with diapycnal diffusivities inferred from dye-spreading (although the dye-spreading included the effect of solitary waves). During late spring the following year, MacKinnon and Gregg (2005) found that dissipation followed the MacKinnon–Gregg scaling but an ε_0 about three times larger ($\varepsilon_0 = 2.0 \times 10^{-9}\,\mathrm{W\,kg^{-1}}$) was required.

The Monterey Bay shelf dissipations were compared to the Gregg–Henyey (3) and MacKinnon–Gregg (5) scalings. Data in the surface and bottom mixed layers as well as that associated with the backscatter features on the shelf south of the canyon were excluded from this analysis. Following MacKinnon and Gregg (2003b) we used first-difference shears calculated from 4-m ADCP bins in both parameterizations. The scattered sampling on the shelf meant it was not practical to calculate low-frequency shears, so 5-min averaged shears were used. Dissipation and stratification were smoothed using an 8-m Bartlett filter and subsampled on to the 4-m depth bins to match the ADCP sampling. Fig. 7 shows dissipation (real and modeled) averaged into logarithmic bins of stratification and shear.

Neither parameterization was good at estimating dissipation in our Monterey Bay measurements. The ε values estimated by the MacKinnon–Gregg scaling (Fig. 7c) were approximately 10 times too small. Even after the constant in (5) was altered to $\varepsilon_0 = 6.1 \times 10^{-9}\,\mathrm{W\,kg^{-1}}$, in order to give the modeled dissipations the same cruise-average as the observed (Fig. 7d), the range of values was smaller than observed ($2.9\times 10^{-9} \leqslant \varepsilon_{MG} \leqslant 1.4 \times 10^{-7}\,\mathrm{W\,kg^{-1}}$ versus $1.6 \times 10^{-10} \leqslant \varepsilon_{observed} \leqslant 7.0 \times 10^{-6}\,\mathrm{W\,kg^{-1}}$). The mean of the Gregg–Henyey scaling was comparable with the observations, and the range was a little larger ($1.0 \times 10^{-11} \leqslant \varepsilon_{GH} \leqslant 1.6\times\ 10^{-6}\,\mathrm{W\,kg^{-1}}$).

When averaged into logarithmic bins, the MacKinnon–Gregg scaling did have the correct functionality with dissipations increasing with increasing shear and increasing stratification (Fig. 7c and d), whereas the Gregg–Henyey dissipations increased with increasing shear and decreasing stratification (Fig. 7b). The functional difference between the two models is consistent with MacKinnon and Gregg (2003b, 2005), and is a direct result of the GM shear assumption (4). Plotting the individual ε_{MG} against $\varepsilon_{observed}$ (Fig. 7f) shows a very weak relationship, unlike the one-to-one relation found on the New England shelf (MacKinnon and Gregg, 2005). No relation existed between $\varepsilon_{observed}$ and ε_{GH} (Fig. 7e).

There are several possible reasons why the MacKinnon–Gregg scaling did not work well for our Monterey Bay shelf data. First, there are significant variations in ε_0. The two sets of observations on the New England shelf (MacKinnon and Gregg, 2003b, 2005) had a similar range of shear-squared values, but although the stratification during the summer was an order of magnitude stronger, the range of ε values was the same. The ε_0 required was three times smaller in summer than spring. Our Monterey Bay observations cover a similar N^2 and S^2 domain as summer New England shelf observations (MacKinnon and Gregg, 2003b), but differences in dissipation levels, result in a nine-fold increase in ε_0. It is conceivable that some of the underlying physics is missing, for example, turbulence on continental shelves may be functionally dependent on local bathymetric slope, as wave scattering from topography can move energy to higher wave numbers.

Second, the 4-m shear scale, used in our analysis and by MacKinnon and Gregg (2003b), may fall in the $\mathbf{k}^{-1}$ rolloff range of the internal wave spectrum and hence not be representative of the internal wave energy level (Gargett, 1990). In the open-ocean thermocline this cutoff occurs at $\mathbf{k} = 0.1$ cpm (cycles per meter), and as the internal wave energy increases the cutoff moves to larger scales. In an attempt to address the effect of the

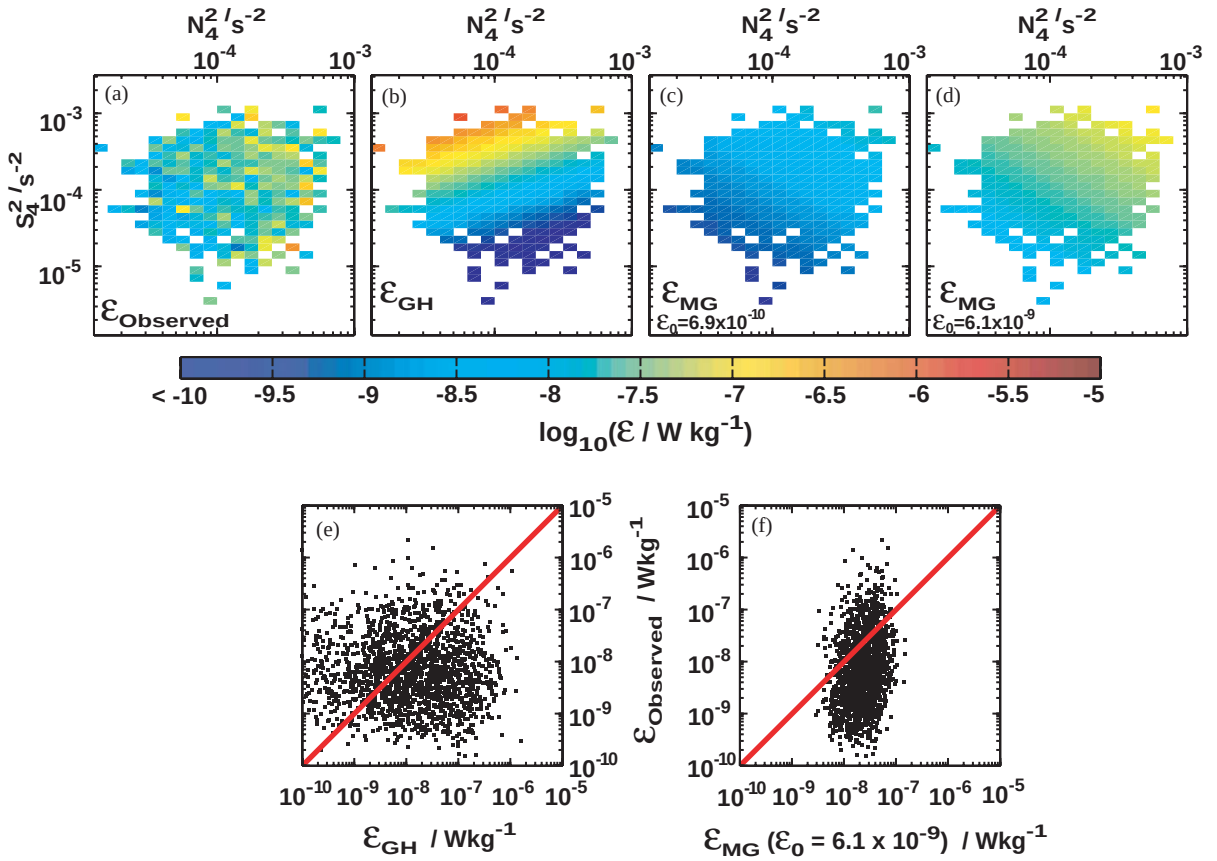

Fig. 7. (a) Observed dissipation data averaged in bins of stratification and shear variance. S_4^2 is the first-difference shear variance calculated from 4-m ADCP depth bins, N_4^2 is the buoyancy frequency filtered to match the ADCP sampling. (b) Gregg–Henyey model dissipation data averaged in bins of stratification and shear variance. (c) Same for the MacKinnon–Gregg scaling with the original empirical constant ($\varepsilon_0 = 6.9 \times 10^{-10}$). (d) Same for MacKinnon–Gregg scaling with $\varepsilon_0 = 6.1 \times 10^{-9}$, derived from matching model and observed averages. (e) and (f) Observed dissipation plotted against modeled ε_{GH} and ε_{MG} ($\varepsilon_0 = 6.1 \times 10^{-9}$) dissipation, respectively.

shear scale, we calculated equivalent 12-m first-difference shears from the 4-m ADCP shears,[3] and repeated the above analysis. The qualitative results remain the same, although the smoother shears and stratifications lead to an even smaller range of dissipations.

A potentially more fundamental problem is that both scalings are based on wave–wave interactions, in which small-scale internal waves are forced towards breaking by interaction with large-scale (e.g. low-mode) shears. Only when the energy is contained in stable low modes are wave–wave interactions expected to dominate turbulence production (MacKinnon and Gregg, 2005). When the energy-containing scales are unstable, shear instabilities dominate and dissipation rates tend to be higher. During internal wave generation or topographical interaction, high modes, which are unstable and dissipate quickly, are created. As our observations were influenced

[3]Twelve-meter velocities are calculated from a 4-m ADCP by $1/9v_i + 2/9v_{i+1} + 3/9v_{i+2} + 2/9v_{i+3} + 1/9v_{i+4}$. The 12-m first-difference shear is then given by $[(1/9v_i + 2/9v_{i+1} + 3/9v_{i+2} + 2/9v_{i+3} + 1/9v_{i+4}) - (1/9v_{i+3} + 2/9v_{i+4} + 3/9v_{i+5} + 2/9v_{i+6} + 1/9v_{i+9})]/12$. Equating this with 4-m first-difference shears implies weighting of 1/27, 3/27, 6/27, 7/27, 6/26, 3/27, and 1/27 to get 12-m shears from 4-m shears.

by local internal tide generation (Section 3), it is possible the energy-containing modes are unstable. Therefore, wave–wave interaction models may not be applicable to this data.

The MacKinnon–Gregg scaling appears to be a reasonable starting point for turbulence parameterization on continental shelves, as it has the correct functional dependence on N and S when averaged into logarithmic bins. However, because the empirical constant ε_0 varies between datasets, some underlying physics may be unaccounted for. Finally we caution that continental shelves may contain regions where any wave–wave interaction-based parameterization may not be valid because different physics dominate.

6. Discussion: nonlinear internal waves

In Section 4.3 we showed the presence of acoustic backscatter features which coincided with elevated turbulent kinetic energy dissipation rates. The exact nature, and certainly the origin of these features is unclear. Possible explanations include biology, dense water gravity flow, or a nonlinear internal wave (NLIW). The airfoil shear probes used to estimate ε are extremely sensitive to impacts with plankton, but as these impacts are no more common in the features than elsewhere it seems unlikely they represent concentrated clouds of biology. The bottom mixed layer in the region of the shelf corresponding to the features was 0.01–0.02 $\mathrm{kg\,m^{-3}}$ lighter than that observed in the adjacent profiles further down the shelf.

In this section, we suggest that these feature are nonlinear internal solitary-like waves. Internal solitary waves are a common feature of the coastal ocean. Waves of depression (downward displacement), which propagate below the surface mixed-layer, are the most commonly observed (e.g. Sandstrom and Oakey, 1995; MacKinnon and Gregg, 2003b; Moum et al., 2003). These can be formed if the layer above the pycnocline is thinner than the deep layer (Liu et al., 1998). When the pycnocline is in the lower half of the water-column, solitary waves will have upward displacement (waves of elevation). Observations of near-bottom waves of elevation have been published for the southern California (Bogucki et al., 1997), Oregon (Klymak and Moum, 2003), and Massachusetts (Scotti and Pineda, 2004) shelves, as well as the continental slope of the Faeroe–Shetland Channel (Hosegood et al., 2004; Hosegood and van Haren, 2004). The relative thickness of the layers above and below the pycnocline can vary along the propagation path, for example, solitary waves have been observed transforming from waves of depression to waves of elevation as they propagated from the South China Sea onto the shelf (Liu et al., 1998; Orr and Mignerey, 2003; Ramp et al., 2004).

The short wavelength of the features means we, unfortunately, lack the high-resolution density and current field observations required to fully describe them as internal solitary waves. The features were observed during the first half of our 22-h cross-canyon survey, when the pycnocline on the southern shelf tended to be just above the bottom mixed-layer allowing for solitary waves of elevation. ADCP velocity measurements reported below indicate that these NLIWs propagated north–westward down the shelf south of the canyon and into the deeper water above the canyon. In agreement with theory, the NLIWs appear to transform from waves of elevation to waves of depression at the canyon rim.

Fig. 8 shows stratification, acoustic backscatter, and velocity data collected over the Monterey Bay shelf south of the canyon during the first across-canyon run. The data shown were taken between 121°52.1′W, 36°46.1′N and 121°52.7′W, 36°47.5′N (approximately 9 km along the canyon axis from Moss Landing), over a 1.5-h period starting at 15:52 15 August. To give as much detail as possible in the narrow features a 90-s averaging interval was used for the velocity (Fig. 8c and d).

6.1. Velocity structure

Although sidelobe interference prevents an ADCP from measuring currents in the bottom 15% of the water column, the top of the tallest wave on the shelf (−1.28 km) was clearly visible in the north velocity record (Fig. 8c). This upper portion of the wave had a north velocity component approaching 0.1 $\mathrm{m\,s^{-1}}$, against a southward

background flow of about $-0.05\,m\,s^{-1}$. The NLIW signature in the east velocity component (Fig. 8d) was less obvious. The observed portion of the tallest wave had an east velocity component of $-0.15\,m\,s^{-1}$ against a background flow of $-0.1\,m\,s^{-1}$.

The three off-shelf features also had corresponding positive v-velocities[4] up to $0.22\,m\,s^{-1}$, against a southward background flow. The westward velocities associated with the off-shelf features at 0.13 and 0.49 km were stronger than the surrounding background flow ($u_{isw} \approx -0.2\,m\,s^{-1}$ versus $u \approx -0.1\,m\,s^{-1}$). The feature 0.99 km from the canyon rim had similar westward velocity to the background.

The velocities within the NLIW measured by the ADCP, allows us to determine the direction of propagation. The NLIWs we observed were propagating north–westward. The ones on the shelf were slightly more west–northwest, while the one furtherest from the canyon rim (0.99 km) was traveling more north–northwest. As the observations were made on the shelf south of the canyon, north–westward velocity implies the NLIWs were propagating downslope towards the canyon. This is opposite to the majority of solitary wave observations to date, both near-surface (e.g. MacKinnon and Gregg, 2003b; Moum et al., 2003; Orr and Mignerey, 2003) and bottom (Klymak and Moum, 2003; Hosegood et al., 2004; Hosegood and van Haren, 2004; Scotti and Pineda, 2004), which propagated towards the coast (upslope). Using mooring data, Bogucki et al. (1997) conclude that the observed bottom solitary wave was propagating across-slope against the background current.

[4]It should be noted that, although these three off-shelf backscatter regions either lead or lag the similarly shaped positive velocity regions, they appear to be manifestations of the same features. The Biosonics acoustic imager points straight down, while the ADCP beams are at 30° from the vertical. The horizontal separation between the Biosonics and ADCP measurement volumes at a depth H is given by $H\sin(30°)$ or about 50 m for a depth of 100 m. This is consistent with the separation observed between Fig. 8b and c. However, as an ADCP assumes homogeneous flow over the area between the beams, the velocities recorded may be biased low.

It is not possible to determine the phase speed of the wave from the particle velocity, however, a sufficiently large wave will break by overturning (Lamb, 2002) requiring the particle velocity to exceed the phase speed (e.g. Orr and Mignerey, 2003; Hosegood and van Haren, 2004). This sets an upper limit on the phase speed of $\approx 0.2\,m\,s^{-1}$ on the shelf and $\approx 0.3\,m\,s^{-1}$ off the shelf (assuming the waves are breaking).

6.2. Waves of elevation

A 330-m section of the Biosonics image (from −1.51 to −1.18 km), which includes the four largest waves of elevation, is plotted with a one-to-one aspect ratio (Fig. 9). These waves were clearly large-scale features with heights approaching half the water column, up to 40 m. The observed horizontal scales were 50–100 m. However, the ship velocity (U_{ship}) throughout this survey was $\sim 0.5\,m\,s^{-1}$ in a similar direction to the waves. Therefore, the actual horizontal scales given by $L_{actual} = L_{observed}(U_{ship} - U_{wave})/U_{ship}$ were shorter than observed. Without knowing the phase speed of the wave we cannot estimate L_{actual}, but using the particle velocity as an upper bound implies that the actual wavelengths are no less that 60% of the observed. These waves are steep, with aspect ratios near one. Near-surface solitary waves of depression usually have much longer horizontal scales and hence smaller aspect ratios (Ostrovsky and Stepanyants, 1989; Orr and Mignerey, 2003). Bottom solitons observed on the Oregon shelf were about 2–4 times wider for similar vertical scales, $L_{actual} \approx 120$ m for a height of 29 m (Klymak and Moum, 2003). Christie et al. (1981) observed similar features in the atmospheric bottom boundary layer over Northern Australia. These waves were up to 400 m high and had associated vertical velocity changes that could exceed $16\,m\,s^{-1}$.

Solitary wave trains evolve to be rank-ordered, as the tallest waves propagate fastest (Osborne and Burch, 1980; Sandstrom and Oakey, 1995). Our observations (Fig. 8), however, show that the second wave (−1.28 km) was the tallest. Other authors have also found solitary wave trains that were not rank-ordered. Orr and Mignerey (2003)

observed that the tallest waves of elevation created from the shoaling waves of depression were in the middle of the train. Ramp et al. (2004) report that solitary wave packets generated by an M_2 tide were not rank-ordered. This lack of rank-order suggests the waves were observed close to their generation sites.

The passage of internal solitary waves displaces isopycnals locally. Unfortunately, undersampling meant we profiled when the wave interface was about the same height above the bed (Fig. 9). (Because of aliasing associated with this undersampling, isopycnals denser than $25\,kg\,m^{-3}$ were not plotted in Fig. 8 for distances < -1 km).

6.3. Transformation to waves of depression

As the NLIWs were traveling north–westward, it follows that the patches of high backscatter and north–westward velocity over the canyon (0.13, 0.49, and 0.99 km in Fig. 8b) were likely NLIWs that propagated off the shelf into deep water. Theoretically, as the thickness of the layer below the pycnocline increases to greater than the surface layer, a solitary wave of elevation will transform to a wave of depression. For these data the transformation should occur near 135-m water depth. Isopycnal displacements within the NLIW observed at 0.13 km, which spans this depth, indicate both upward and downward displacement.

Although our sampling was not designed to observe these NLIWs, we were fortunate to have AMP profiles through the features at 0.13 and 0.49 km. Fig. 10 plots selected isopycnals (spaced $0.01\,kg\,m^{-3}$ apart) over the acoustic backscatter image.

We first consider the wave at 0.49 km (Fig. 10). The 25.98-$kg\,m^{-3}$ isopycnal (contoured in purple) was fairly horizontal, whereas the isopycnals within the NLIW ($\sigma_\theta = 25.99-26.01\,kg\,m^{-3}$) were displaced downward compared to neighboring profiles. The 26.01-$kg\,m^{-3}$ isopycnal was 4.7 m deeper than the neighboring onshore profile and 6.1 m deeper than the neighboring offshore profile. This local downward isopycnal displacement classifies this feature as a wave of depression, which is in line with theory as the pycnocline base was at 80 in 230 m of water.

The NLIW at 0.13 km was more complicated. The 25.95-$kg\,m^{-3}$ isopycnal (contoured in red) was nearly horizontal through this wave. Lighter isopycnals (25.91–25.94 $kg\,m^{-3}$) were displaced upward within the NLIW compared to neighboring profiles. However, denser isopycnals (25.96–25.98 $kg\,m^{-3}$) were displaced downward. We believe this mixed isopycnal signature (upward and downward displacement) was because of the significant water depth changes associated with the canyon rim. The leading edge of the NLIW was in 150 m of water, while the trailing edge was in 120 m. With the pycnocline between 55 and 80 m (Fig. 8a), theory would predict a wave of depression at the leading edge, and a wave of elevation at the trailing edge. Therefore, we appear to have observed a NLIW transforming from a wave of elevation to a wave of depression as it propagated into deeper water.

The transition from wave of elevation to wave of depression occurs over a shorter horizontal scale than the transformation from waves of depression to waves of elevation observed on the South China Sea shelf (Orr and Mignerey, 2003). This difference in scale may be due to the significantly steeper slope of the canyon wall (0.17) compared to the South China Sea shelf (0.016), or could be due to a fundamental difference in the transition mechanism between the two directions. In particular, the waves of elevation have a considerably shorter wavelength as they approach the transition point than the waves of depression.

6.4. Role in sediment transport

The most intense acoustic backscatter was on the leading edge of the waves propagating across the shelf (Fig. 9). Within the NLIWs, the backscatter intensity was considerably lower (Fig. 9). Although we have no independent verification, the intense backscatter likely includes resuspended sediments. The mooring data of Bogucki et al. (1997) showed a marked increase in beam attenuation coefficient (a measure of turbidity) coinciding with the leading edge of the observed internal solitary wave. Klymak and Moum (2003) found elevated 880 nm optical backscatter corresponding

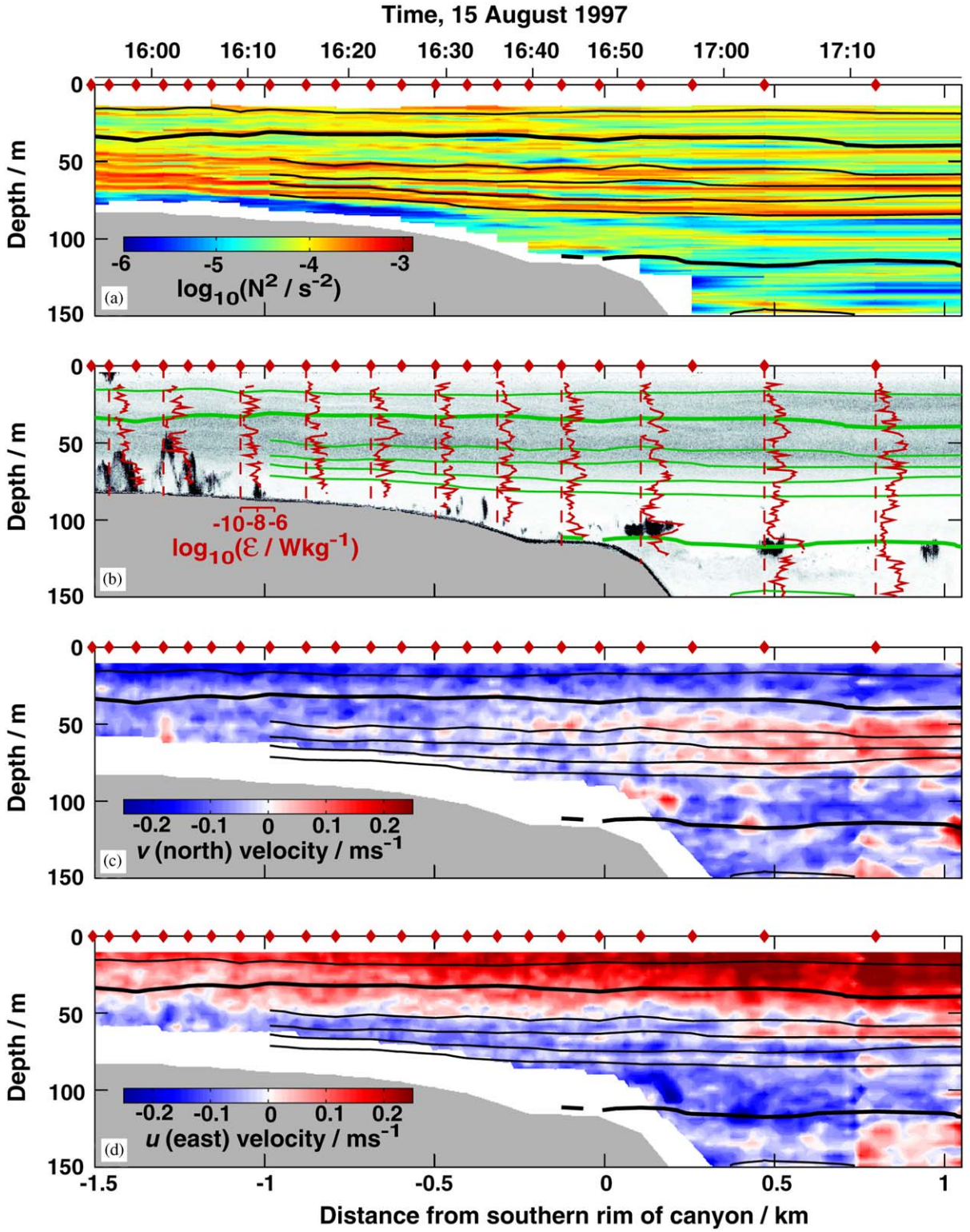
Time, 15 August 1997
16:00
16:10
16:20
16:30
16:40
16:50
17:00
17:10
Depth / m
0
50
100
150
-6
-5
-4
-3
log10(N2 / s-2)
(a)
-10-8-6
log10(ε / Wkg-1)
(b)
-0.2 -0.1 0 0.1 0.2
v (north) velocity / ms-1
(c)
-0.2 -0.1 0 0.1 0.2
u (east) velocity / ms-1
(d)
-1.5
-1
-0.5
0
0.5
1
Distance from southern rim of canyon / km

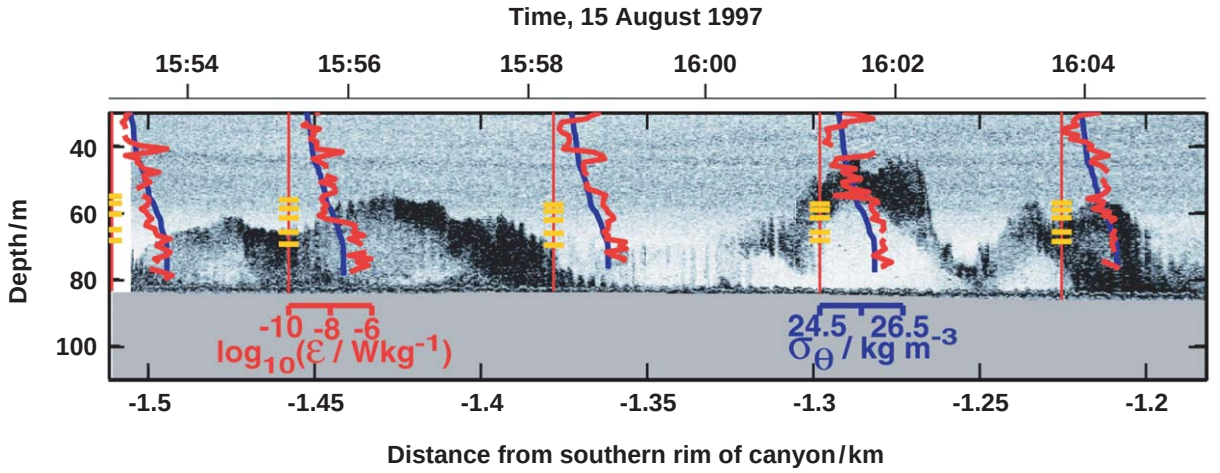

Fig. 9. A 330-m section including the main solitary-like wave features on the southern shelf observed during the first cross-canyon run (see Fig. 8b). This figure is plotted with a one-to-one aspect ratio. Dissipation rates and density are overplotted for AMP profiles 16536–16540, the exact profile locations are uncertain within ~5 m. The short horizontal lines mark the depth of the $\sigma_\theta = 25.4, 25.5, 25.6, 25.7$, and $25.8\,\mathrm{kg\,m^{-3}}$ isopycnals.

to resuspended fine silt and clay within a solitary wave train. Using sediment traps Hosegood et al. (2004) found the daily sediment flux increased more than 100-fold after the passage of a solitary wave train. They describe a 'rotor' with upward velocities at the leading edge of the solitary wave, which eroded the surface layer and exposed the underlying nutrient rich sediment.

Interestingly, the bottom NLIW located between −1.37 and −1.45 km had a discernable ellipse-shaped region of lower backscatter at its center, completely surrounded by high backscatter. This may indicate a trapped core, which is a possible nonlinear solitary wave solution (Lamb, 2003; Klymak and Moum, 2003), and would greatly increase transport of fluids and particles.

Strong sediment resuspension associated with near-bottom NLIWs of elevation, combined with propagation into the canyon, may be an efficient mechanism for removing sediment from the Monterey Bay shelf. Below the NLIWs at 0.13 and 0.49 km there was increased backscatter suggestive of entrained sediments settling out (Fig. 10).

6.5. Generation

It is unclear where the observed downslope-propagating bottom NLIWs were generated. Generally, coastal internal solitary waves are formed by nonlinear steepening of internal waves propagating from a shelf break generation region (Sandstrom and Oakey, 1995), or by distantly generated internal waves propagating over the shelf break (Small, 2003). The resulting solitary waves propagate upslope towards the coast. Alternative mechanisms include internal solitary waves generated by and propagating upstream away from critical flow over a topographic feature (Melville and Helfrich, 1987; Bogucki et al., 1997),

Fig. 8. Data over the southern shelf from the first cross-canyon run (15:52 to 17:17, 15 August 1997). (a) Stratification, (b) acoustic backscatter, (c) v (north) velocity, and (d) u (east) velocity. The high backscatter regions are associated with north–westward propagating nonlinear internal waves (see text). Panel b has dissipation rate profiles overlayed for selected profiles. Isopycnals between $\sigma_\theta = 24.8$ and $26.2\,\mathrm{kg\,m^{-3}}$ are overlayed in $0.2\text{-kg\,m}^{-3}$ intervals on each panel, the heavier lines are $\sigma_\theta = 25$ and $26\,\mathrm{kg\,m^{-3}}$. (Isopycnals greater than $25\,\mathrm{kg\,m^{-3}}$ are not plotted between −1.5 and −1 km because of aliasing.) Along the top of each panel, the positions of the AMP profiles 16537–16557 are marked.

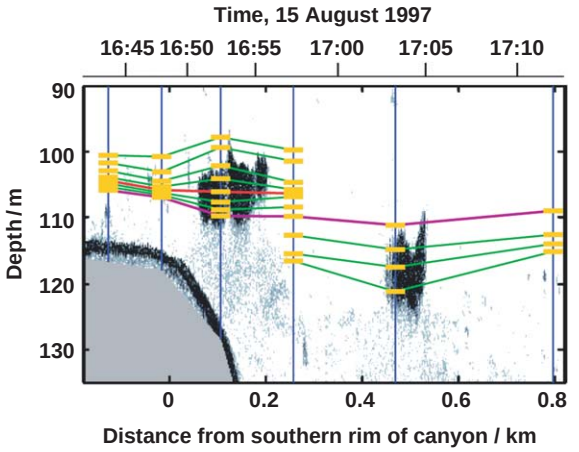

Fig. 10. Two nonlinear internal waves that propagated off the shelf into deep water over the canyon (see Fig. 8b). The vertical lines mark the location of AMP profiles 16552–16557. Horizontal lines mark the depth of selected isopycnals spaced 0.01 kg m^{-3} apart. For the wave feature at 0.13 km, the range of plotted isopycnals is between 25.91 and 25.98 kg m^{-3}, and for the 0.49-km feature the isopycnal range is 25.98–26.01 kg m^{-3}. The red line is $\sigma_\theta = 25.95$ kg m^{-3}, and the purple line is 25.98 kg m^{-3}.

and the release of standing lee waves (Apel et al., 1997). In a two-layer laboratory experiment Helfrich (1992) observed that when shoaling NLIWs broke they could produce turbulent vortices or boluses of dense water. These boluses then propagated upslope until dissipated by friction.

A number of authors have determined a tidal source for the internal solitary waves they observed (e.g. Osborne and Burch, 1980; Small, 2003; Ramp et al., 2004), while others stress the importance of atmospheric forcing (e.g. Hosegood and van Haren, 2004). Twelve across-canyon survey runs were performed in a 22-h period, of which nine collected data on the shelf south of the canyon. The largest and most pronounced NLIWs (Fig. 8b) occurred near lower-high tide (Fig. 1c). Observations during the following ebb showed only small isolated near-bed backscatter. Near higher-low tide, a train of three high backscatter regions were observed just off the canyon rim. Of the remaining runs, acoustic images were only available for the last two, by which time the pycnocline had shallowed and no NLIWs were observed. Therefore, our acoustic backscatter data constitutes a very short time-series (≈ 6 h) and does not allow us to comment on a possible tidal origin for the NLIWs.

North–westward propagation, and the absence of rank-ordering implies that the generation site was close by and towards shore. A NLIW of depression, from a shelf break or offshore generation site, which broke near shore to produce

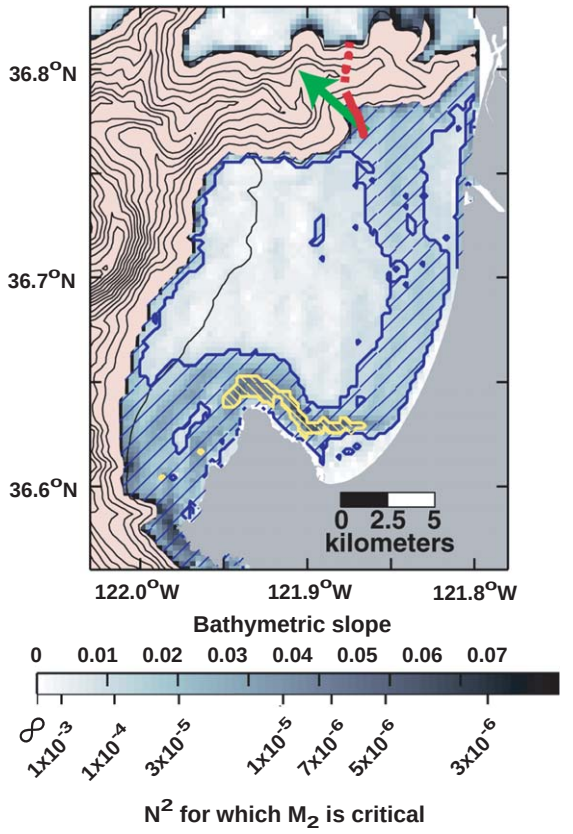

Fig. 11. Bathymetric slopes on the continental shelf, calculated as $\sqrt{(\Delta z/\Delta x)^2 + (\Delta z/\Delta y)^2}$ on an ≈ 275-m $\times$ 275-m grid. The solid red line gives the location of the sampling line shown in Fig. 8, and the dashed line gives the remainder of the across-canyon survey line. The north–westward propagation direction of the nonlinear internal waves is shown by the green arrow. The stratifications (N^2) required to make the bathymetry critical at the M_2 tidal frequency are given below the color bar. The mapping of bathymetric slope to critical stratification is nonlinear (6). The blue cross-hatching shows supercritical bathymetry for $N^2 = 10^{-4}$ s^{-2}, and the yellow shows supercritical bathymetry for $N^2 = 10^{-5}$ s^{-2}.

NLIWs of elevation or boluses could be consistent with our observations. Tim Stanton (Naval Postgraduate School, Monterey; pers. comm., 2005) has observed this NLIW breaking in 12 m of water at the southern end of the bay.

Direct local generation is also a possibility. Whether or not the bathymetry can generate an internal tide depends on the characteristic slope (α), which in turn depends on stratification (N^2) and the latitude via

$$\alpha = \sqrt{\frac{\omega^2 - f^2}{N^2 - \omega^2}}, \tag{6}$$

where ω is the wave frequency and f is the Coriolis frequency. Fig. 11 shows the bathymetric slope on the Monterey Bay shelf south of the canyon. The largest tidal component in Monterey Bay is the lunar semi-diurnal (Petruncio et al., 1998), therefore, we shall assume the M_2 tide to be the likely source for tidally driven NLIW wave generation. The stratifications required to make the shelf bathymetry critical for an M_2 tide are given in Fig. 11. Observed near-bottom stratification ranged from $N^2 = 10^{-6}$ to $10^{-3}\,s^{-2}$, resulting in significant spatial and temporal variability of potential sites for M_2 internal tide generation. With $N^2 = 10^{-6}\,s^{-2}$, which was observed concurrently with the NLIWs on the shelf (Fig. 8), the entire shelf south of the canyon is subcritical. Assuming a near-bottom stratification of $10^{-4}\,s^{-2}$, which was sometimes observed on the southern shelf away from the influence of the NLIWs, gives a swath of supercritical bathymetry nearly parallel to the coast (blue cross-hatching in Fig. 11), including upslope of the observed NLIWs.

One of the major outstanding questions of this research is where, when, and how these nonlinear solitary-like waves were generated. Larger scale observations, both spatially and temporally, would be required to answer this.

7. Summary

- Acoustic and microstructure data were collected on the continental shelf within and at the mouth of Monterey Bay as part of a 2-week experiment focused on the canyon head (Carter and Gregg, 2002) and a submarine fan (Lien and Gregg, 2001). Spatially, the shelf data fall into four regions, all within 4 km of the shelf break or canyon rim. These shelf regions tended to be part of longer survey lines, resulting in irregular temporal coverage.
- The majority of the variance in the velocity field observed, both at the mouth and within the bay, was consistent with a propagating internal tide. Over half of our observations showed counterclockwise rotation with depth (upward energy propagation), but those near low water contained a mixture of upward and downward propagation. The complex bathymetry seems to allow the barotropic tide to generate a baroclinic tide deep on the submarine fan or canyon. As the barotropic tide passes over the shelf break/canyon rim, a second internal tide is generated. On the shelf, the internal wave field was primarily dominated by the locally generated internal tide but contained energy from the surface reflection of the more distantly generated internal tide.
- Average turbulent kinetic energy dissipation rates at the four sites were $7.4–55.8 \times 10^{-9}\,W\,kg^{-1}$ and diapycnal diffusivities were $6.1–37.8 \times 10^{-5}\,m^2\,s^{-1}$. These values are elevated above observations made over continental shelves with no significant topographical variation, but less than many observations affected by topographic features. The close proximity of the shelf break and canyon rim, locally generated internal tides, and nonlinear internal waves all contribute to the elevated turbulence.
- Considerable temporal and spatial variability was observed. There was a factor of five difference in $\bar{\varepsilon}$ and $\overline{K_\rho}$ between two sites 5 km apart on the shelf north of the canyon. The lower mixing occurred near neap tide and with stratification consistent with coastal upwelling, while the higher mixing was a week later after the upwelling event had passed. On the shelf south of the canyon, 20% of the observed dissipation was associated with nonlinear internal waves of elevation. In the upper 150 m above the canyon and adjacent to the southern

canyon rim, almost half the observed dissipation was associated with nonlinear internal waves.

- The open-ocean scaling of shear variance and stratification to dissipation (Gregg, 1989), as well as a recently developed shelf scaling (MacKinnon and Gregg, 2003b), were compared to our microstructure observations with the nonlinear internal waves excluded. Neither scaling estimated the dissipation on the Monterey shelf well. The MacKinnon–Gregg model had the correct functional dependence on N and S, i.e. dissipation increased with increasing shear and increasing stratification. The empirical constant ε_0 required to give the same averaged model dissipation as observed was nine times that given by MacKinnon and Gregg (2003b). This may suggest some underlying physics is missing. The proximity of our observations to an internal tide generation region, where unstable locally generated high modes can be expected to contain energy, meant the wave–wave interaction mechanisms underlying these parameterizations may not be dominant locally.
- An unexpected, but important finding was the existence of what we believe to be downslope-propagating nonlinear internal solitary-like waves. Large-amplitude near-bottom waves of elevation were observed propagating north–westward across the shelf south of the canyon. These high-aspect-ratio waves had vertical scales up to 40 m. Once they reached the canyon rim they propagated into deep water, transforming into waves of depression. Acoustic backscatter images suggest that sediment entrained by the waves of elevation on the shelf settles out over the canyon. Turbulent kinetic energy dissipation rates in the solitary-like waves are elevated compared to the local background levels. Average ε levels were higher in the waves of depression compared to the waves of elevation.

Further observations will be required to understand the processes involved in this complex coastal mixing environment.

Acknowledgements

We are grateful to Jack Miller, Earl Krause, Gordy Welsh, Jen MacKinnon, Jody Klymak, and the crew of R/V Point Sur for assistance in data collection. Discussions with Dave Winkel, Eric Kunze, Jen Mackinnon, Matthew Alford, Jody Klymak, Oliver Fringer, and two anonymous reviewers were helpful. This research was funded by the National Science Foundation grant OCE9633067.

References

Apel, J.R., Badiey, M., Chiu, C.-S., Finette, S., Headrick, R., Kemp, J., Lynch, J.F., Newhall, A., Orr, M.H., Pasewark, B.H., Tielbuerger, D., Turgut, A., von der Heydt, K., Wolf, S., 1997. An overview of the 1995 SWARM shallow-water internal wave acoustic scattering experiment. IEEE Journal of Oceanic Engineering 22 (3), 465–500.

Baines, P.G., 1982. On internal tide generation models. Deep-Sea Research 29 (3A), 307–338.

Bogucki, D., Dickey, T., Redekopp, L.G., 1997. Sediment resuspension and mixing by resonantly generated internal solitary waves. Journal of Physical Oceanography 27 (7), 1181–1196.

Breaker, L.C., Broenkow, W.W., 1994. The circulation of Monterey Bay and related processes. In: Ansell, A.D., Gibson, R.N., Barnes, M. (Eds.), Oceanography and Marine Biology: An Annual Review, vol. 32. UCL Press, pp. 1–64.

Carter, G.S., Gregg, M.C., 2002. Intense, variable mixing near the head of Monterey Submarine Canyon. Journal of Physical Oceanography 32 (11), 3145–3165.

Christie, D.R., Muirhead, K.J., Clarke, R.H., 1981. Solitary waves in the lower atmosphere. Nature 293 (5827), 46–49.

Egbert, G.D., Ray, R.D., 2000. Significant dissipation of tidal energy in the deep ocean inferred from satellite altimeter data. Nature 405, 775–778.

Gargett, A.E., 1990. Do we really know how to scale the turbulent kinetic energy dissipation rate ε due to breaking of oceanic internal waves? Journal of Geophysical Research 95 (C9), 15971–15974.

Garrett, C.J.R., Munk, W.H., 1972. Space-time scales of internal waves. Geophysical and Astrophysical Fluid Dynamics 2, 225–264.

Garrett, C.J.R., Munk, W.H., 1975. Space-time scales of internal waves: a progress report. Journal of Geophysical Research 80, 291–297.

Gill, A.E., 1982. Atmosphere–Ocean Dynamics. Academic Press, New York 662pp.

Gregg, M.C., 1989. Scaling turbulent dissipation in the thermocline. Journal of Geophysical Research 94 (C7), 9686–9698.

Gregg, M.C., Özsoy, E., 1999. Mixing on the Black Sea shelf north of the Bosphorous. Geophysical Research Letters 26 (13), 1869–1872.

Gregg, M.C., Winkel, D.P., Mackinnon, J.A., Lien, R.-C., 1999. Mixing over shelves and slopes. In: Müller, P., Henderson, D. (Eds.), Dynamics of oceanic internal gravity waves II, Proceedings, Hawaiian Winter Workshop, January 18–22, 1999. University of Hawaii at Manoa, pp. 35–42.

Helfrich, K.R., 1992. Internal solitary wave breaking and run-up on a uniform slope. Journal of Fluid Mechanics 243, 133–154.

Henyey, F.S., Wright, J., Flatté, S.M., 1986. Energy and action flow through the internal wave field: an eikonal approach. Journal of Geophysical Research 91, 8487–8495.

Holloway, P.E., Merrifield, M.A., 1999. Internal tide generation by seamounts, ridges, and islands. Journal of Geophysical Research 104 (C11), 25,937–25,951.

Horne, E.P., Loder, J.W., Naime, C.E., Oakey, N.S., 1996. Turbulence dissipation rates and nitrate supply in the upper water column on Georges Bank. Deep-Sea Research II 43 (7–8), 1683–1712.

Hosegood, P., van Haren, H., 2004. Near-bed solibores over the continental slope in the Faeroe–Shetland Channel. Deep-Sea Research II 51, 2943–2971.

Hosegood, P., Bonnin, J., van Haren, H., 2004. Solibore-induced sediment resuspension in the Faeroe–Shetland Channel. Geophysical Research Letters 31, L09301.

Klymak, J.M., Moum, J.N., 2003. Internal solitary waves of elevation advancing on a shoaling shelf. Geophysical Research Letters 30 (20), 2045.

Kunze, E., Rosenfeld, L.K., Carter, G.S., Gregg, M.C., 2002. Internal waves in Monterey Submarine Canyon. Journal of Physical Oceanography 32 (6), 1890–1913.

Lamb, K.G., 2002. A numerical investigation of solitary internal waves with trapped cores formed via shoaling. Journal of Fluid Mechanics 451, 109–144.

Lamb, K.G., 2003. Shoaling solitary waves: on a criterion for the formation of waves with trapped cores. Journal of Fluid Mechanics 478, 81–100.

Leaman, K.D., Sanford, T.B., 1975. Vertical energy propagation of inertial waves: a vector spectral analysis of velocity profiles. Journal of Geophysical Research 80 (15), 1975–1978.

Ledwell, J.R., Duda, T.F., Sundermeyer, M.A., Seim, H.E., 2004. Mixing in a coastal environment, Part I: a view from dye dispersion. Journal of Geophysical Research 109 (C10), C10013.

Lien, R.-C., Gregg, M.C., 2001. Observations of turbulence in a tidal beam and across a coastal ridge. Journal of Geophysical Research 106 (C3), 4575–4591.

Liu, A.K., Chang, Y.S., Hsu, M.-K., Liang, N.K., 1998. Evolution of nonlinear internal waves in the East and South China Seas. Journal of Geophysical Research 103 (C4), 7995–8008.

MacKinnon, J.A., Gregg, M.C., 2003a. Shear and baroclinic energy flux on the summer New England shelf. Journal of Physical Oceanography 33 (7), 1462–1475.

MacKinnon, J.A., Gregg, M.C., 2003b. Mixing on the late-summer New England shelf—solibores, shear and stratification. Journal of Physical Oceanography 33 (7), 1476–1492.

MacKinnon, J.A., Gregg, M.C., 2005. Spring mixing: turbulence and internal waves during restratification on the New England shelf. Journal of Physical Oceanography, accepted for publication.

Melville, W.K., Helfrich, K.R., 1987. Transcritical two-layer flow over topography. Journal of Fluid Mechanics 178, 31–52.

Moum, J.N., Farmer, D.M., Smyth, W.D., Armi, L., Vagle, S., 2003. Structure and generation of turbulence at interfaces strained by internal solitary waves propagating shoreward over the continental shelf. Journal of Physical Oceanography 33 (10), 2093–2112.

Munk, W., 1997. Once again: once again—tidal friction. Progress Oceanography 40 (1), 7–35.

Nash, J.D., Moum, J.N., 2001. Internal hydraulic flows on the continental shelf: high drag states over a small bank. Journal of Geophysical Research 106 (C3), 4593–4611.

Orr, M.H., Mignerey, P.C., 2003. Nonlinear internal waves in the South China Sea: observation of the conversion of depression internal waves to elevation internal waves. Journal of Geophysical Research 108 (C3), 3064.

Osborne, A.R., Burch, T.L., 1980. Internal solitons in the Andaman Sea. Science 208 (4443), 451–460.

Osborn, T.R., 1980. Estimates of the local rate of vertical diffusion from dissipation measurements. Journal of Physical Oceanography 10, 83–89.

Osborn, T.R., Crawford, W.R., 1980. An airfoil probe for measuring turbulent velocity fluctuations in water. In: Dobson, F., Hasse, L., Davis, R. (Eds.), Air–Sea Interaction: Instruments and Methods. Plenum Press, New York, pp. 369–386.

Ostrovsky, L.A., Stepanyants, Y.A., 1989. Do internal solitons exist in the ocean? Review of Geophysics 27 (3), 293–310.

Petruncio, E.T., Rosenfeld, L.K., Paduan, J.D., 1998. Observations of the internal tide in Monterey Canyon. Journal of Physical Oceanography 28 (10), 1873–1903.

Pingree, R.D., New, A.L., 1989. Downward propagation on internal tidal energy into the Bay of Biscay. Deep-Sea Research 36 (5), 735–758.

Prinsenberg, S.J., Rattray Jr., M., 1975. Effects of continental slope and variable Brunt–Väisälä frequency on the coastal generation of internal tides. Deep-Sea Research 22, 251–263.

Prinsenberg, S.J., Wilmot, W.L., Rattray Jr., M., 1974. Generation and dissipation of coastal internal tides. Deep-Sea Research 21, 263–281.

Ramp, S.R., Tang, D., Duda, T.F., Lynch, J.F., Liu, A.K., Chiu, C.-S., Bahr, F., Kim, H.-R., Yang, Y.J., 2004. Internal solitons in the Northeastern South China Sea part I: sources and deep water propagation. IEEE Journal of Ocean Engineering 29 (4), 1157–1181.

Rosenfeld, L.K., Schwing, F.B., Garfield, N., Tracy, D.E., 1994. Bifurcating flow from an upwelling center: a cold

water source for Monterey Bay. Continental Shelf Research 14 (9), 931–964.

Rudnick, D.L., Boyd, T.J., Brainard, R.E., Carter, G.S., Egbert, G.D., Gregg, M.C., Holloway, P.E., Klymak, J.M., Kunze, E., Lee, C.M., Levine, M.D., Luther, D.S., Martin, J.P., Merrifield, M.A., Moum, J.N., Nash, J.D., Pinkel, R., Rainville, L., Sanford, T.B., 2003. From tides to mixing along the Hawaiian Ridge. Science 301, 355–357.

Sandstrom, H., Oakey, N.S., 1995. Dissipation in internal tides and solitary waves. Journal of Physical Oceanography 25 (4), 604–614.

Scotti, A., Pineda, J., 2004. Observation of very large and steep internal waves of elevation near the Massachusetts coast. Geophysical Research Letters 31, L22307.

Sharples, J., Moore, C.M., Abraham, E.R., 2001. Internal tide dissipation, mixing, and vertical nitrate flux at the shelf edge of NE New Zealand. Journal of Geophysical Research 106 (C7), 14069–14081.

Shea, R.E., Broenkow, W.W., 1982. The role of internal tides in nutrient enrichment of Monterey Bay, California. Estuarine, Coastal and Shelf Science 15 (1), 57–66.

Simpson, J.H., Crawford, W.R., Rippeth, T.P., Campbell, A.R., Cheok, J.V.S., 1996. The vertical structure of turbulent dissipation in shelf seas. Journal of Physical Oceanography 26 (8), 1579–1590.

Small, J., 2003. Refraction and shoaling of nonlinear internal waves at the Malin Shelf break. Journal of Physical Oceanography 33 (12), 2657–2674.

Sundermeyer, M.A., Ledwell, J.R., 2001. Lateral dispersion over the continental shelf: analysis of dye release experiments. Journal of Geophysical Research 106 (C5), 9603–9621.

Wesson, J.C., Gregg, M.C., 1994. Mixing at Camarinal Sill in the Strait of Gibraltar. Journal of Geophysical Research 99, 9847–9878.